OXFORD

Human Molecular Genetics, 2016, Vol. 25, No. 7 1434–1446

doi: 10.1093/hmg/ddw025
Advance Access Publication Date: 28 January 2016
Original Article

ORIGINAL ARTICLE

Genetic and pharmacological evidence implicates cathepsins in Niemann-Pick C cerebellar degeneration

Chan Chung[1], Prasanth Puthanveetil[1], Daniel S. Ory[2] and Andrew P. Lieberman[1,*]

[1]Department of Pathology, University of Michigan Medical School, Ann Arbor, MI 48109, USA and [2]Diabetic Cardiovascular Disease Center and Department of Internal Medicine, Washington University School of Medicine, St Louis, MO 63110, USA

*To whom correspondence should be addressed at: Department of Pathology, University of Michigan Medical School, 3510 MSRB1, 1150 W. Medical Center Dr., Ann Arbor, MI 48109-0605, USA. Tel: +1 7346474624; Fax: +1 7346153441; Email: liebermn@umich.edu

Abstract

Niemann-Pick C1 (NPC) disease, an autosomal recessive lipid trafficking disorder caused by loss-of-function mutations in the *NPC1* gene, is characterized by progressive neurodegeneration resulting in cognitive impairment, ataxia and early death. Little is known about the cellular pathways leading to neuron loss. Here, we studied the effects of diminishing expression of cystatin B, an endogenous inhibitor of cathepsins B, H and L, on the development of NPC neuropathology. We show that decreased expression of cystatin B in patient fibroblasts enhances cathepsin activity. Deletion of the encoding *Cstb* gene in Npc1-deficient mice resulted in striking deleterious effects, particularly within the cerebellum where diffuse loss of Purkinje cells was observed in young mice. This severe pathology occurred through cell autonomous mechanisms that triggered Purkinje cell death. Moreover, our analyses demonstrated the mislocalization of lysosomal cathepsins within the cytosol of Npc1-deficient Purkinje cells. We provide evidence that this may be a consequence of damage to lysosomal membranes by reactive oxygen species (ROS), leading to the leakage of lysosomal contents that culminates in apoptotic cell death. Consistent with this notion, toxicity from ROS was attenuated in an NPC cell model by cystatin B over-expression or pharmacological inhibition of cathepsin B. The observation that *Npc1* and *Cstb* deletion genetically interact to potently enhance the degenerative phenotype of the NPC cerebellum provides strong support for the notion that lysosomal membrane permeabilization contributes to cerebellar degeneration in NPC disease.

Introduction

Lysosomes are critical components of the cellular degradation machinery and important nodes in the homeostatic response to metabolic demands (1). These organelles degrade macromolecules delivered to them through vesicular trafficking or autophagy by the action of a family of acidic hydrolases including proteases, lipases, nucleases, glycosidases, phospholipases, phosphatases and sulfatases (2). More than 50 diseases related to lysosomal dysfunction, many caused by enzyme deficiencies, have been identified since the discovery of this organelle in the mid-twentieth century (3).

Lysosomal proteases, or cathepsins, are required for the housekeeping function of these organelles in protein turnover. These cathepsins have been implicated in a variety of human diseases, including neurodegenerative disorders (4–6). Cathepsins are classified by their catalytic mechanism into aspartic, serine, threonine, metallo or cysteine proteases (7). Cysteine cathepsins, the largest family of lysosomal proteases, are synthesized as inactive precursors and are activated by cleavage in the acidic environment of the lysosome (8). Although it was initially thought that lysosomal cysteine proteases are unstable and rapidly inactivated outside the lysosome, a number of studies have established that

Received and Revised: January 11, 2016. **Accepted:** January 25, 2016

cysteine cathepsins are stable and partially active at neutral pH, such as within the cytoplasm (9–11). Indeed, accumulating evidence suggests that the release of cathepsins into the cytosol triggers apoptotic cell death (12). A first line of self-defense in preventing apoptosis initiated through this mechanism is provided by intracellular inhibitors of cysteine proteases, the cystatins. Cystatin B, which inhibits cathepsins B, L and H, is a reversible and competitive inhibitor of these proteases (13). As such, cystatin B is poised to play an important role in limiting the activation of apoptosis in situations in which cells are exposed to a variety of toxic challenges that impact lysosomal membrane integrity.

Here we tested the extent to which cystatin B regulates neurodegeneration in Niemann-Pick type C (NPC) disease, an autosomal recessive disorder characterized by progressive cognitive decline, seizures, dystonia, abnormal eye movements and early death (14). The cause of NPC disease is loss-of-function mutations in the *NPC1* or *NPC2* genes (15,16), whose protein products act cooperatively in the efflux of cholesterol from late endosomes and lysosomes (17,18). In NPC disease, the accumulation of unesterified cholesterol and glycosphingolipids in late endosomes and lysosomes is associated with impairments of cellular proteostasis, including abnormalities in autophagy (19–22), accumulation of ubiquitinated proteins (23–25) and impairment of lysosomal cathepsin activity (6). These abnormalities correlate with the occurrence of severe neurodegeneration that is characterized, in part, by the loss of cerebellar Purkinje neurons. However, little is known about the cellular pathways leading to neurodegeneration in this disorder.

In this study, we present evidence that cystatin B is a potent modifier of cerebellar degeneration in NPC mice. We show that knockdown of cystatin B markedly increases cathepsin activity in NPC1-deficient fibroblasts and that deletion of the encoding *Cstb* gene enhances cerebellar degeneration in *Npc1*−/− mice. This accentuation of NPC neuropathology is shown to be neuron autonomous and due to enhanced apoptotic death of Purkinje cells. Our findings uncover an important pathway that regulates neuron loss in the NPC brain and suggest that damage to organelle membranes by reactive oxygen species (ROS) may be a significant contributor to disease.

Results

Cystatin B knockdown increases cathepsin activity in NPC1 patient fibroblasts

Previous studies have implicated the leakage of lysosomal cathepsins into the cytosol as a contributing event in the neurodegeneration that occurs in Niemann-Pick disease (26,27). Here, we sought to test this hypothesis by relieving the activity of cystatin B, an endogenous inhibitor of cathepsins B, H and L that has been shown to regulate enzymatic activity in models of cancer and neurodegenerative disease (28–30). To accomplish this, we diminished expression of cystatin B (CSTB) in NPC1 patient fibroblasts by transfecting *CSTB*-targeted siRNA. Cathepsin B activity in live cells was monitored using Magic Red, a fluorophore covalently bound to a di-arginine peptide motif. Prior to cleavage, Magic Red is cell permeable and non-fluorescent. After it is cleaved by cathepsin B in lysosomes, the dye fluoresces red. The rate of fluorescence accumulation was quantified and used to estimate cathepsin B activity *in situ*. In accordance with prior studies (6), we found that cathepsin B activity in primary fibroblasts from NPC1 patients was reduced to approximately half of controls (Fig. 1A). Cystatin B knockdown in NPC1-deficient cells increased cathepsin B activity to the level of unaffected controls (Fig. 1A). This enhancement of enzymatic B activity was associated with diminished cystatin B expression (Fig. 1B). In contrast, we observed no change in the expression or maturation of cathepsin B. In addition, we observed no change in NPC1 protein expression (Fig. 1B) or in the accumulation of filipin-positive unesterified cholesterol (Fig. 1C). We concluded that diminishing cystatin B expression in NPC1-deficient cells increased cathepsin activity without altering cholesterol storage.

Cystatin B deletion exacerbates NPC cerebellar degeneration

We next determined whether enhanced cathepsin activity resulting from cystatin B deletion modified the disease phenotype in a mouse model of NPC. To accomplish this, we generated *Npc1* null mice that were deficient in cystatin B. Mice with a cystatin B null allele were previously generated to model progressive myoclonic epilepsy of the Unverricht–Lundborg type. These mice begin to develop disease around 6 months of age, which includes loss of cerebellar granule neurons, but not Purkinje cells. At earlier time points, between 1 and 3 months, mutants are normal in body size, weight, behavior and histopathology when compared with wild-type littermates (31). We therefore generated *Npc1* and *Cstb* double null mice and focussed our analysis on young animals. Unexpectedly, these double null mutants were generated at a very low frequency. Of the 101 *Cstb*−/− pups generated from multiple matings of *Npc1*+/−, *Cstb*+/− adults, only 4% were homozygous for the *Npc1* null allele. By χ^2 analysis, only double null mutants (*Npc1*−/−, *Cstb*−/−) were derived from these matings at a frequency that was significantly lower than expected ($P < 0.001$; Table 1).

We observed a striking enhancement of the NPC phenotype in mice that were deficient in cystatin B. As early as 4 weeks of age, double null mutants showed marked deficits in body and liver weight when compared with *Npc1* nulls that were haploinsufficient or wild-type for cystatin B (Fig. 2A). We were unable to train these young double null mutants to cross a balance beam (data not shown), a motor task that is sensitive to Purkinje cell loss in Npc1-deficient animals (32). This severe, early onset behavioral impairment prompted us to perform histological examination of the brains of these mice and littermate controls at 4 weeks of age. Remarkably, the double null mutants contained virtually no cerebellar Purkinje cells, except for only rare neurons in lobule X (Fig. 2B). At this age, there was no detectable Purkinje cell loss in either anterior or posterior cerebellar lobules of *Npc1* or *Cstb* single null mutants. The loss of Purkinje cells in lobule X is particularly noteworthy as these neurons are typically resistant to toxic effects of *Npc1* deficiency, even in animals aged to 6 months (32). The paucity of calbindin-positive Purkinje cells in anterior and posterior cerebellar lobules of double null mutants was associated with marked astrocytic and microglial reaction (Fig. 2C and D). In contrast, cystatin B deficiency did not exacerbate accumulation of the ganglioside GM2 or unesterified cholesterol in the brains of Npc1-deficient mice (Fig. 2E and F), suggesting that mechanisms other than enhanced lipid storage led to the worsened phenotype. These analyses indicated that there was a genetic interaction between *Npc1* and *Cstb* deficiency that markedly increased the severity of neuropathology.

Although our initial studies focussed on cerebellar Purkinje cells, they left unanswered whether other brain regions in *Npc1*-deficient mice showed enhanced pathology in the setting of *Cstb* deletion. To begin to address this question, we stained midline sagittal brain sections for glial fibrillary acidic protein (GFAP) as reactive astrocytes are sensitive indicators of damage in the central nervous system (CNS). We observed marked gliosis

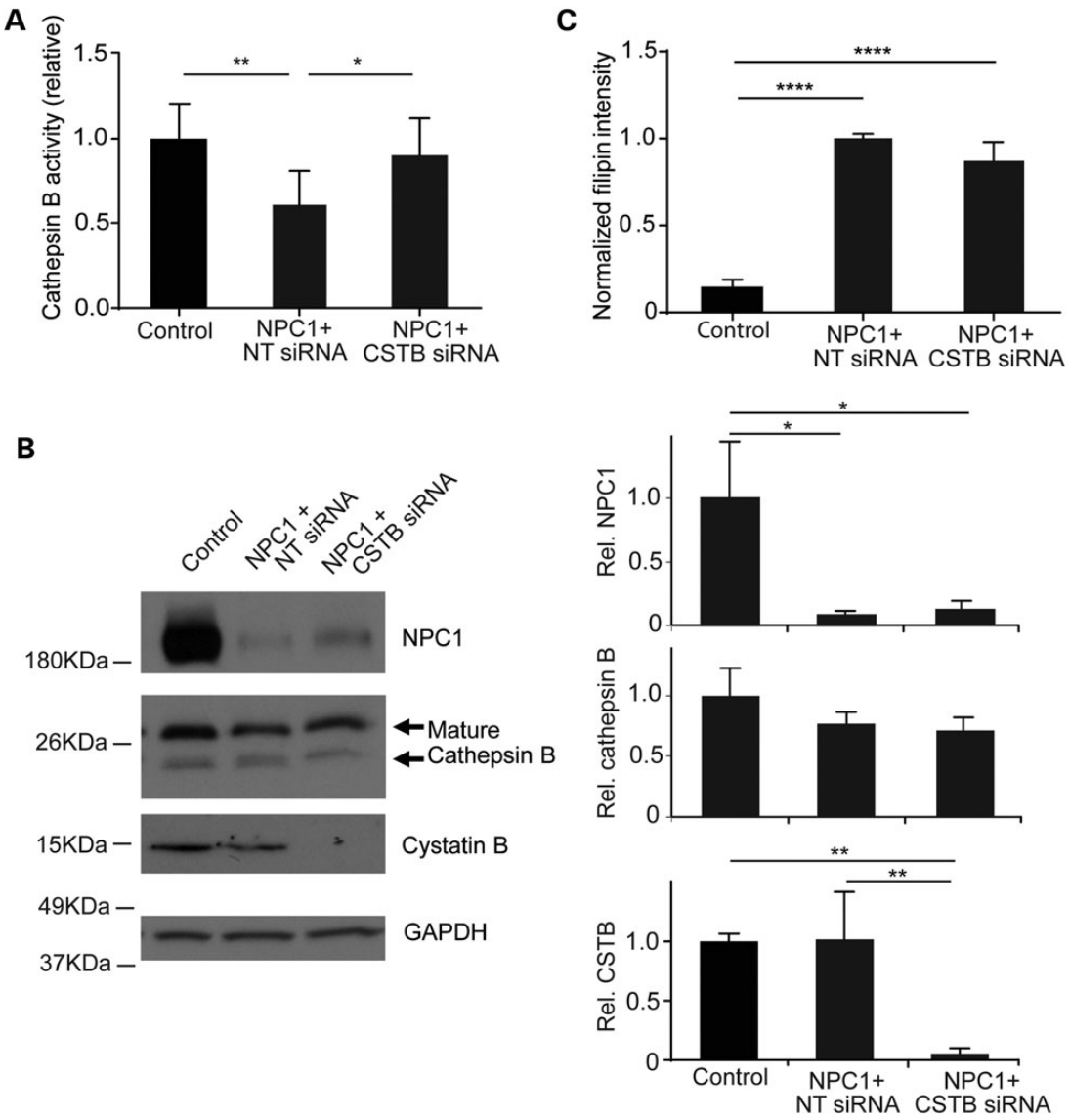

Figure 1. Cystatin B knockdown increases cathepsin B activity in NPC1 patient fibroblasts. Control fibroblasts and NPC1-deficient fibroblasts treated with non-targeted siRNA (NT siRNA) or cystatin B siRNA (CSTB siRNA) for 48 h were analyzed. (**A**) Relative cathepsin B activity. Data are mean ± SD, $n = 3$ independent experiments, $^{*}P < 0.05$ and $^{**}P < 0.01$. (**B**) Left panel, western blot of the expression of NPC1, cathepsin B, cystatin B and GAPDH. Right panel, NPC1, cathepsin B and cystatin B intensity relative to GAPDH (mean ± SD, $n = 3$, $^{*}P < 0.05$ and $^{**}P < 0.01$). (**C**) Unesterified cholesterol was stained by filipin and quantified across three independent experiments. Data are mean ± SD, $n = 40$–50 fields of cells per group in total, $^{****}P < 0.0001$.

Table 1. Npc1 genotype frequency of Cstb−/− and Cstb+/+ mice

Npc1 genotype	Expected ratio	*Cstb*+/+ background, N = 130 Observed	*Cstb*−/− background, N = 101 Observed
Npc1+/+	1	31	18
Npc1+/−	2	72	79
Npc1−/−	1	27	4
χ^2		1.75	36.05*

*Statistically significant. χ^2 for two degrees of freedom for a *P*-value of 0.05 is 5.99.

that was largely restricted to the cerebellum and was only seen in double null mutants at 4 weeks of age (Fig. 3A–D). This gliosis was associated with significant cerebellar atrophy (Fig. 3E), which reflected the extensive loss of Purkinje neurons, the main output neurons of the cerebellum. Our findings indicate that deletion of the *Cstb* gene resulted in marked cerebellar atrophy and gliosis in young *Npc1*-deficient mice.

Cystatin B deficiency triggers enhanced, cell autonomous Purkinje cell degeneration

These findings led us to determine whether cystatin B deficiency exacerbated cerebellar degeneration in a cell autonomous manner. To address this question, we generated *Cstb*−/− mice that were deficient in *Npc1* only in Purkinje cells by using a previously characterized conditional null allele (32). Cre recombinase driven by the *Pcp2* promoter resulted in transgene expression in Purkinje cells that initiated around postnatal day 6 and was present in all Purkinje cells by postnatal days 14–21 (33). Therefore, this

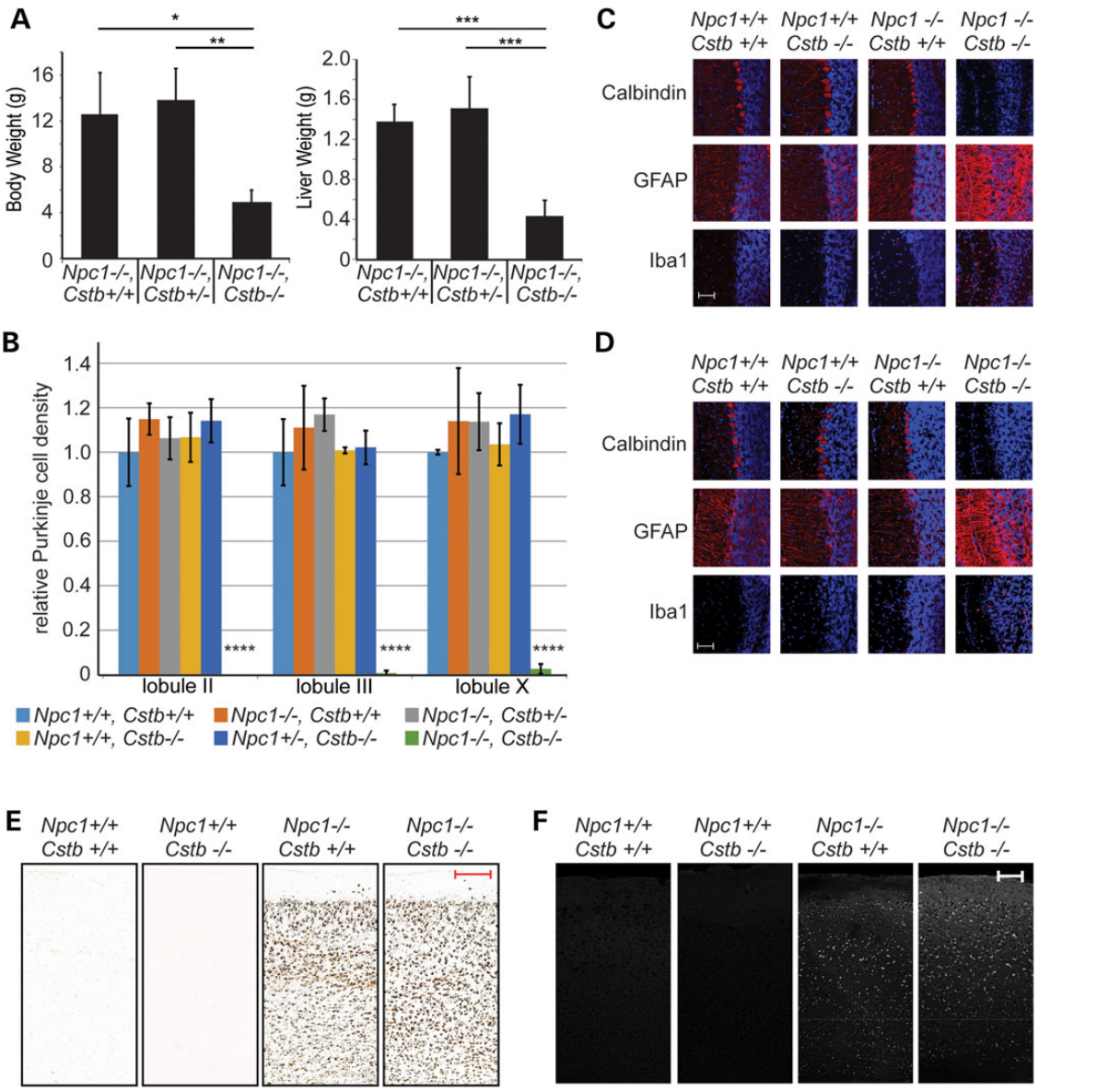

Figure 2. Phenotype of *Npc1*, *Cstb* null mice. (**A**) Body weight, at left, and liver weight, at right, of mice at 4 weeks of age (mean ± SD, $n = 3$–6 mice per genotype, $^{*}P < 0.05$, $^{**}P < 0.01$ and $^{***}P < 0.001$). (**B**) Purkinje cell density in midline cerebellar sections at 4 weeks of age (mean ± SD, $n = 3$ mice per genotype, $^{****}P < 0.0001$). (**C** and **D**) Immunofluorescence staining (red) for Purkinje cells (calbindin), astrocytes (GFAP) and microglia (Iba1) in cerebellar lobule III (C) and lobule X (D). Nuclei are stained with DAPI. Scale bar = 50 μm. (**E**) Immunohistochemical staining of cerebral cortex for GM2 at 4 weeks of age. Scale bar = 200 μm. (**F**) Filipin staining of cerebral cortex at 4 weeks of age. Scale bar = 100 μm.

strategy enabled post-developmental and cell-type-restricted deletion of *Npc1*.

At 8 weeks of age, partial Purkinje cell loss restricted to anterior cerebellar lobules was detected in *Npc1 Flox/-*, *Pcp2-Cre*, *Cstb+/+* mice, as reported previously (32). In contrast, strikingly few Purkinje cells were observed in anterior and posterior cerebellar lobules of *Npc1 Flox/-*, *Pcp2-Cre* mice that were deficient in cystatin B (Fig. 4A and B). Quantification confirmed that cystatin B deficiency significantly diminished soma size of Purkinje cells remaining in lobule X (Fig. 4C) and enhanced neuron loss in anterior and posterior cerebellar lobules (Fig. 4D). This exacerbation of Purkinje cell loss in *Npc1 Flox/-*, *Pcp2-Cre*, *Cstb−/−* mice impacted the disease phenotype as it led to impaired motor function as measured by balance beam performance (Fig. 4E).

The paucity of Purkinje cells in adult double null mutant mice could reflect either a neurodevelopmental impairment or neurodegeneration. To distinguish between these possibilities, we examined Purkinje cell density in 3-week-old *Npc1 Flox/-*, *Pcp2-Cre*, *Cstb−/−* mice (Fig. 5A). These young mutants showed Purkinje neurons in all cerebellar lobules, although at a density that was lower than *Npc1 Flox/-*, *Pcp2-Cre*, *Cstb+/+* controls. A comparison of Purkinje cell density in *Npc1 Flox/-*, *Pcp2-Cre*, *Cstb−/−* mice at 3 and 8 weeks of age revealed an age-dependent loss of neurons (Fig. 5B). This was associated with the occurrence of Purkinje cells that stained for activated caspase-3 in the cerebellum of 3-week-old *Npc1 Flox/-*, *Pcp2-Cre*, *Cstb−/−* mice (Fig. 5C). We conclude that cystatin B deficiency triggered apoptotic death of Purkinje neurons in young Npc1-deficient mice.

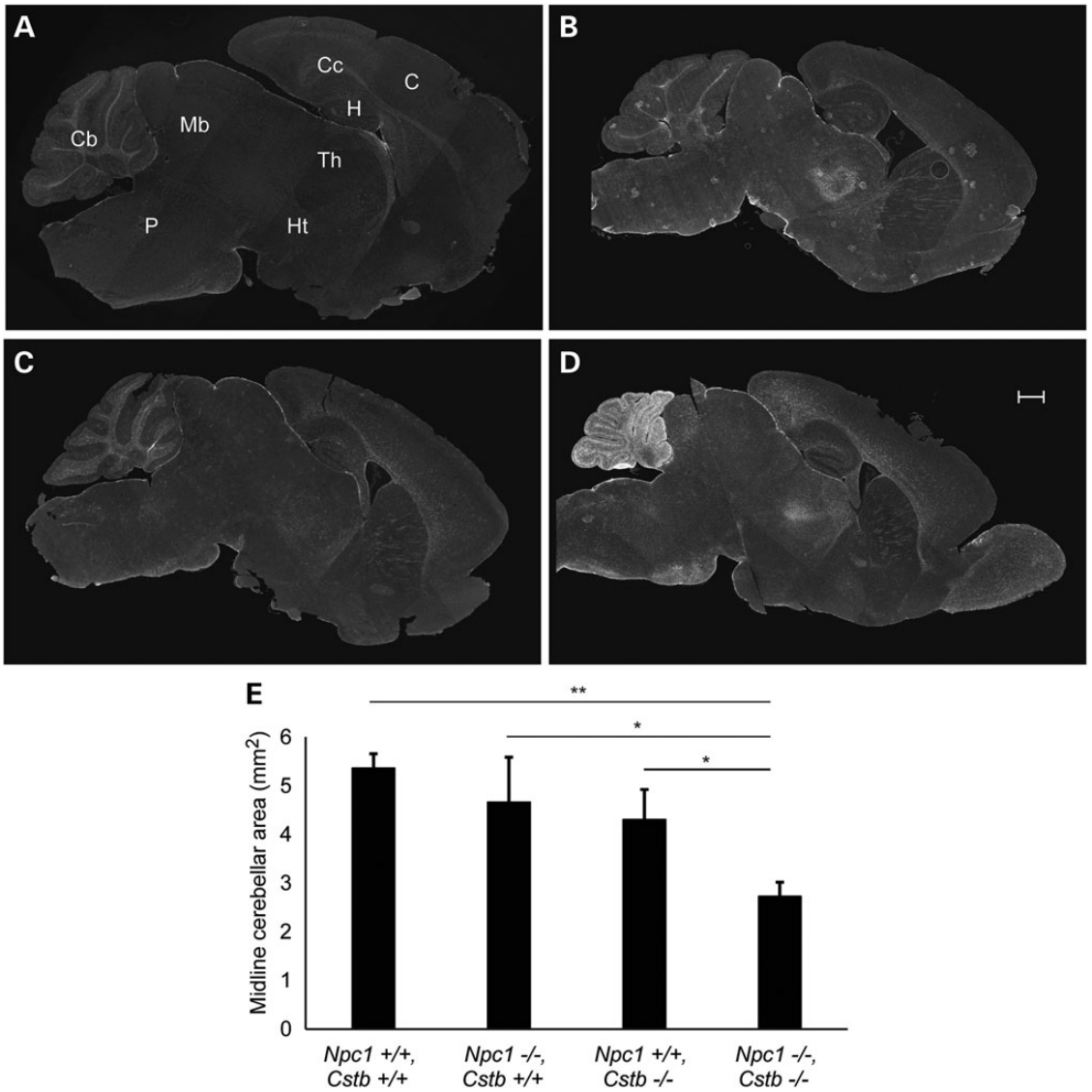

Figure 3. The cerebellum of *Npc1*, *Cstb* null mice is markedly gliotic and atrophic. Midline brain sections of mice at 4 weeks of age were stained by immunofluorescence for GFAP. (**A**) *Npc1*+/+, *Cstb*+/+, (**B**) *Npc1*−/−, *Cstb*+/+, (**C**) *Npc1*+/+, *Cstb*−/− and (**D**) *Npc1*−/−, *Cstb*−/−. Cb, cerebellum; Mb, midbrain; P, pons; C, cerebral cortex; Cc, corpus callosum; H, hippocampus; Th, thalamus; Ht, hypothalamus. Scale bar = 500 μm. (**E**) Quantification of cerebellar area in midline sections (mean ± SD, $n = 3$ per genotype, $^{*}P < 0.05$ and $^{**}P < 0.01$).

Npc1 deficiency disrupts cathepsin localization in cerebellar Purkinje cells

To explore the mechanism by which cystatin B deficiency enhanced cerebellar degeneration in NPC mice, we considered the possibility that cathepsins were partially mislocalized outside lysosomes in the Npc1-deficient mouse brain, rendering Purkinje cells sensitive to cystatin B deletion and leading to apoptosis. This notion was based on prior work showing that cathepsin B is markedly increased in cytosolic fractions of cerebellar lysates from Npc1-deficient mice compared with controls (26). Furthermore, the release of cathepsins into the cytosol has been shown to trigger cell death in other model systems (12). To determine cathepsin localization in Npc1-deficient Purkinje cells, we performed immunofluorescence staining for cathepsins B or L and LAMP-1, a marker of late endosomes and lysosomes (Fig. 6). Confocal microscopy demonstrated that the majority of the cathepsin signal in the cytosol of Purkinje cells co-localized with Lamp1 in *Npc1 Flox*/+, *Pcp2-Cre* mice, irrespective of the *Cstb* genotype. In contrast, co-localization of cathepsins with LAMP1 was significantly diminished in *Npc1*−/− Purkinje cells. These data indicated that the disease was associated with an increased fraction of cathepsins outside LAMP1-positive vesicles, consistent with previous observations (26). Similar findings have been reported in a mouse model of Niemann-Pick type A (NPA) disease, a related neurodegenerative disorder caused by deficiency of acid sphingomyelinase (27). Notably, the mislocalization of cathepsins in *Npc1*−/− Purkinje cells was not influenced by *Cstb* genotype, suggesting that cystatin B deficiency exerted effects on disease phenotype by modulating cathepsin activity rather than localization.

Enhanced cytoplasmic localization of cathepsins could reflect leakage of lysosomal contents due to organelle membrane damage. Indeed, prior studies have indicated that lysosomal membrane permeabilization triggers cell death and that this can occur after damage by ROS (34–37). Analysis of the *Npc1*−/−

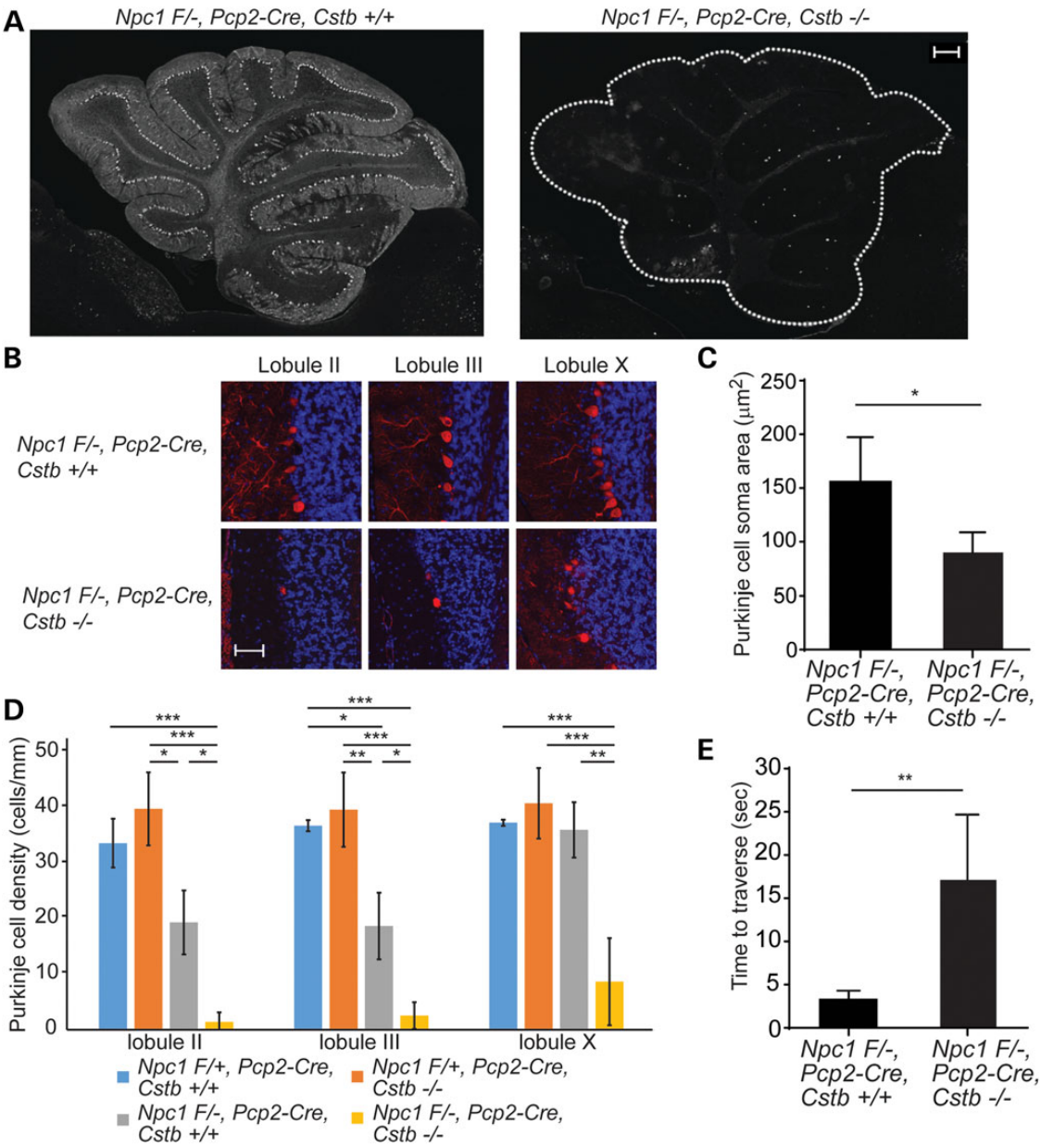

Figure 4. Enhanced Purkinje cell loss following cystatin B deficiency is cell autonomous. (**A**) Immunofluorescence staining for Purkinje cells (calbindin antibody) at 8 weeks of age in the cerebellar midline. Left panel, *Npc1 F/-*, *Pcp2-Cre*, *Cstb+/+*; right panel, *Npc1 F/-*, *Pcp2-Cre*, *Cstb−/−*. Scale bar = 200 μm. (**B**) Immunofluorescence staining for calbindin (red) in cerebellar lobules II, III and X; nuclei were stained by DAPI. Scale bar = 50 μm. (**C**) Quantification of Purkinje cell soma area (mean ± SD, $n \geq 45$ cells per genotype, $^{*}P < 0.05$). (**D**) Purkinje cell density in lobules II, III and X was quantified in the cerebellar midline (mean ± SD, $n = 4$ mice per genotype, $^{*}P < 0.05$, $^{**}P < 0.01$ and $^{***}P < 0.001$). (**E**) Balance beam performance at 8 weeks of age (mean ± SD, $n \geq 3$ mice per genotype, $^{**}P < 0.01$).

mouse brain has demonstrated the occurrence of oxidative damage (38,39), and lipid oxidation products have emerged as a sensitive biomarker of NPC disease (40). Moreover, treatment of Npc1 mice with the antioxidant N-acetylcysteine results in a mild suppression of the disease phenotype (41). Consistent with these observations, we found that cerebellar Purkinje cells deficient in Npc1 exhibited substantially more staining for superoxide dismutase 2 (SOD2) than controls, irrespective of the *Cstb* genotype (Fig. 7A). Similarly, NPC1 patient fibroblasts showed a significant increase in the generation of ROS when compared with the control fibroblasts (Fig. 7B).

These observations prompted us to study the sensitivity of control and NPC1 patient fibroblasts to cytotoxicity induced by ROS. This approach is based on published studies demonstrating that ROS can trigger cell death by promoting lysosomal membrane permeabilization (34–37). We used hydrogen peroxide as an oxidative stressor as it easily crosses membranes and induces formation of reactive hydroxyl and iron-centered radicals (42). These free radicals destabilize the lysosomal membrane and induce lysosomal membrane permeabilization-dependent cell death (42–44). As shown in Figure 7C, NPC1-deficient fibroblasts were significantly more sensitive to cytotoxicity induced by hydrogen peroxide than control fibroblasts, with mean lethal concentration 50 (LC_{50}) values in NPC1-deficient and control cells of 337.9 μM (95% confidence interval 316.0–361.3) and 486.8 μM (95% confidence interval 465.4–509.1), respectively.

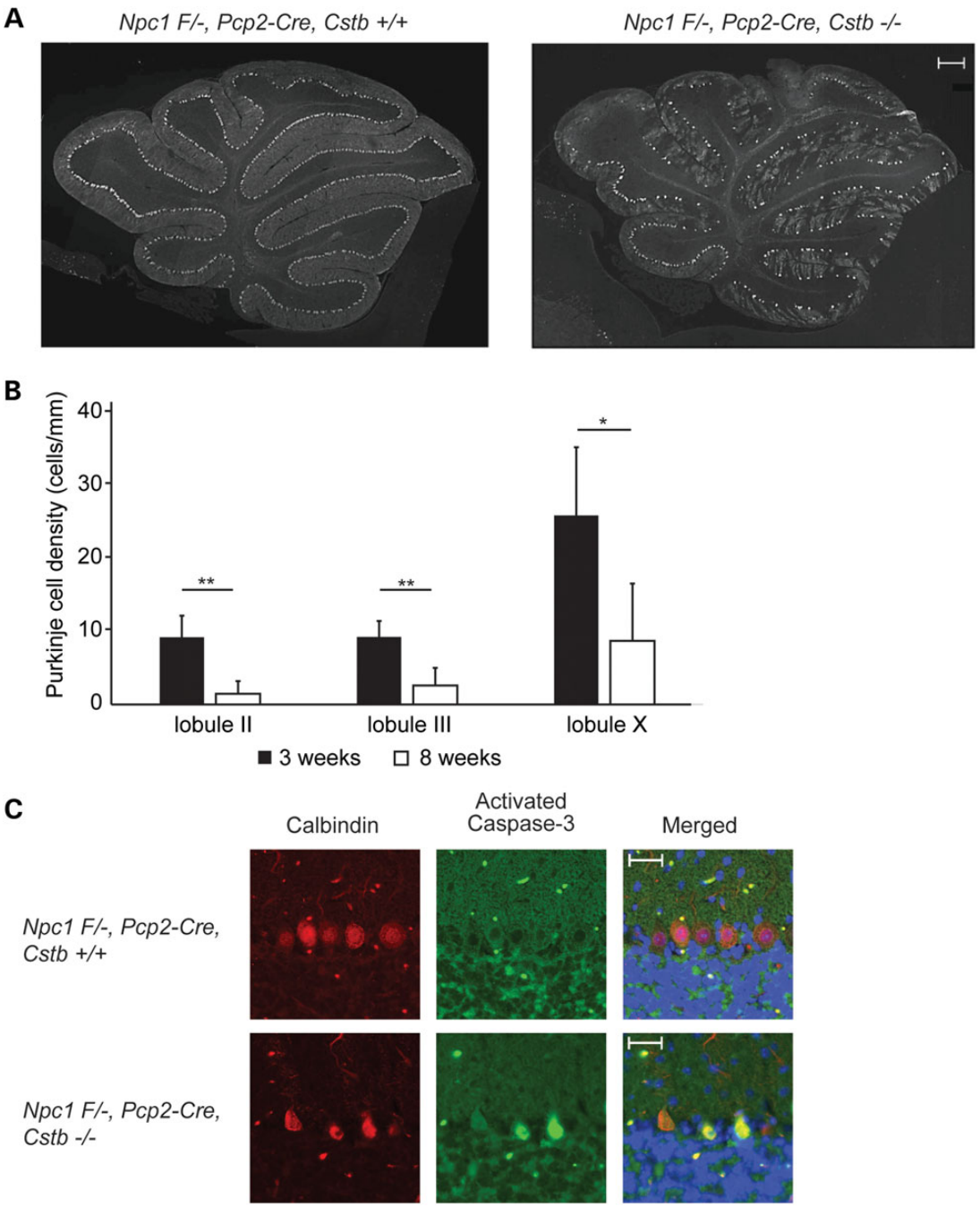

Figure 5. Purkinje cell loss following cystatin B deficiency is due to neurodegeneration and not a neurodevelopmental deficiency. (**A**) Immunofluorescence staining of Purkinje cells (calbindin antibody) at 3 weeks of age in the cerebellar midline. Left panel, *Npc1 F/-, Pcp2-Cre, Cstb+/+*; right panel, *Npc1 F/-, Pcp2-Cre, Cstb−/−*. Scale bar = 200 μm. (**B**) Purkinje cell density in lobules II, III and X was quantified in the cerebellar midline of 3-week-old *Npc1 F/-, Pcp2-Cre, Cstb−/−* mice; data from 8-week-old *Npc1 F/-, Pcp2-Cre, Cstb−/−* mice (from Fig. 4C) are shown for comparison (mean ± SD, $n = 4$, $^{*}P < 0.05$ and $^{**}P < 0.01$). (**C**) Detection of apoptotic Purkinje cells by co-immunofluorescence staining for calbindin (red) and activated caspase-3 (green) at 3 weeks of age in the cerebellar midline; nuclei were stained by DAPI. Top panel, *Npc1 F/-, Pcp2-Cre, Cstb+/+*; bottom panel, *Npc1 F/-, Pcp2-Cre, Cstb−/−*. Scale bar = 50 μm.

To determine the extent to which cathepsins contributed to the cytotoxicity of NPC1-deficient cells exposed to hydrogen peroxide, we used genetic and pharmacological approaches to diminish cathepsin activity. Cystatin B over-expression rendered NPC1-deficient cells significantly more resistant to hydrogen peroxide-induced cell death (Fig. 7D). Similarly, treatment with CA-074 methyl ester (CA-074ME), which is a selective, irreversible and membrane-permeable cathepsin B inhibitor (45–47), significantly increased cell viability following exposure to hydrogen peroxide (Fig. 7E). Taken together, these data indicate that cathepsin activity contributes to the susceptibility of NPC1-deficient cells to ROS-mediated cytotoxicity. This conclusion is supported by the results of a 3-week treatment trial of NPC mice with the cathepsin inhibitor E64d, a cysteine protease inhibitor that inhibits cathepsins B, H and L as well as calpain (52–54). We used E64d for these experiments as CA-074ME

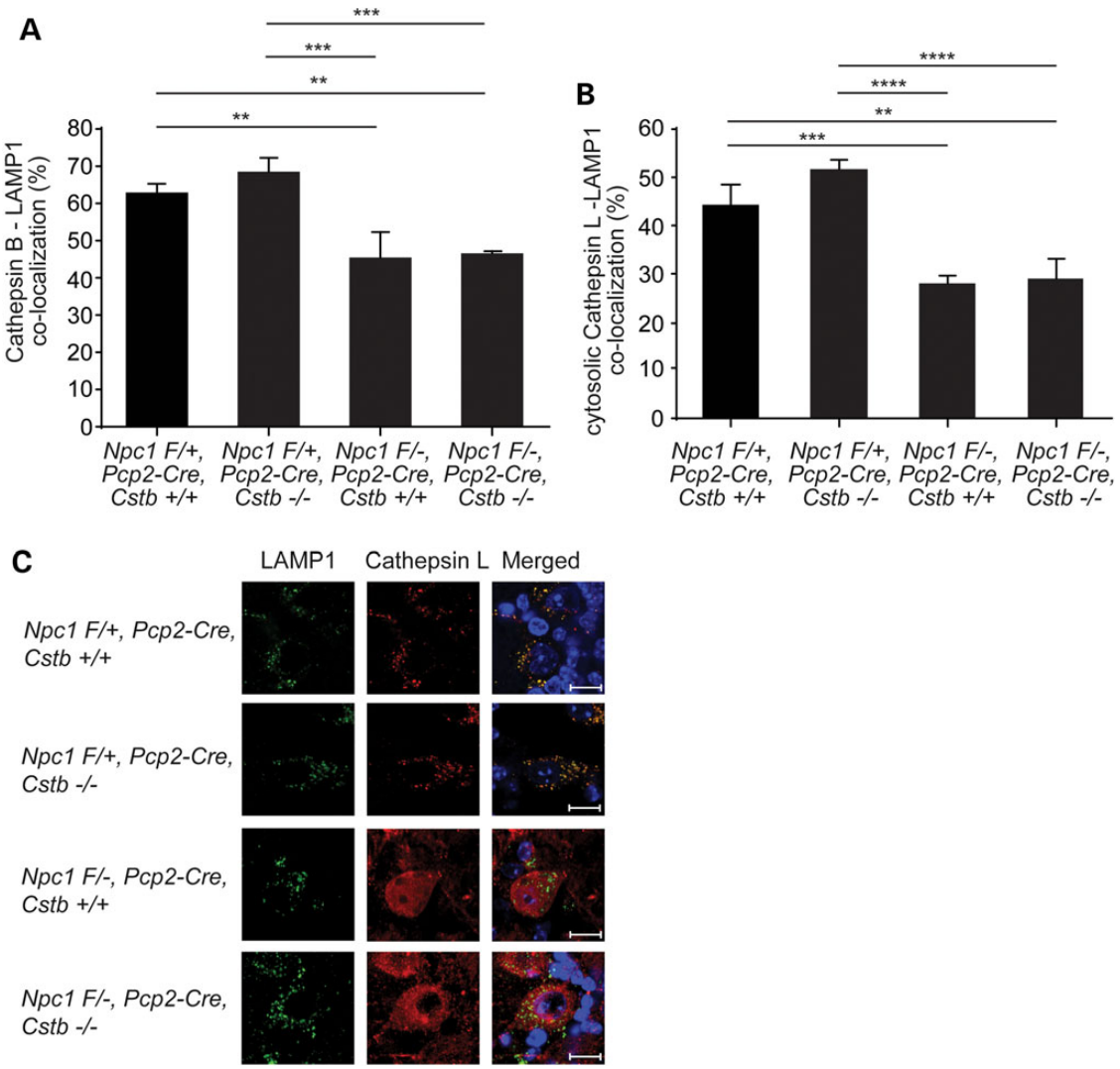

Figure 6. Cathepsin mislocalization in *Npc1*-deficient Purkinje cells. Co-localization of cathepsin B or L with LAMP1 was examined in midline cerebellar sections of mice at 8 weeks of age. Co-localization of cathepsin B (**A**) or cytosolic cathepsin L (**B**) with LAMP1 was quantified (mean ± SD, $n = 10$ cells, pooled from three independent experiments, $^{**}P < 0.01$, $^{***}P < 0.001$ and $^{****}P < 0.0001$). (**C**) Representative immunofluorescence staining for LAMP1 (green) and cathepsin L (red) is shown; nuclei were stained by DAPI. Scale bar = 10 μm.

exhibits poor brain penetration following peripheral delivery (48–51). We treated *Npc1-1061T* homozygous mice (61) by daily oral gavage, starting at 7 weeks of age. Treatment corresponded with the onset of behavioral impairment and Purkinje cell loss in this model (61). Analysis of Purkinje cells in sagittal sections of the cerebellar midline at 10 weeks of age revealed a significant rescue of soma size (Fig. 7F), but no change in cell number. These findings are consistent with the modest effects of N-acetylcysteine treatment in symptomatic NPC1-deficient mice that were previously reported (41) and support a model in which lysosomal membrane permeabilization is a component of the cascade leading to neuron loss in the NPC cerebellum.

Discussion

The pathways leading to the severe neurodegeneration that occurs in the NPC brain have remained elusive. Here, we demonstrate that cystatin B, an endogenous inhibitor of lysosomal cathepsins B, L and H, plays a critical role in regulating Purkinje cell degeneration in NPC mice. We show that decreased expression of cystatin B in patient fibroblasts enhances cathepsin activity. Deletion of the encoding *Cstb* gene in Npc1-deficient mice results in markedly deleterious effects, particularly within the cerebellum where diffuse loss of Purkinje cells is observed. This severe pathology is shown to occur through cell autonomous mechanisms that trigger apoptotic Purkinje cell death. Moreover, our analyses corroborate data in the literature, showing that lysosomal cathepsins are mislocalized within the cytosol of Npc1-deficient Purkinje cells (26,27). We provide evidence that this may be a consequence of damage to lysosomal membranes by ROS, leading to the leakage of lysosomal contents that culminates in neurodegeneration (Fig. 8). The observation that *Npc1* and *Cstb* deletion genetically interact to potently enhance the degenerative phenotype of the NPC cerebellum provides strong support for this proposed pathogenic mechanism.

This model of disease takes into account the observation that Npc1 deficiency does not alter cathepsin maturation, a process that is dependent on normal trafficking to lysosomes. Moreover,

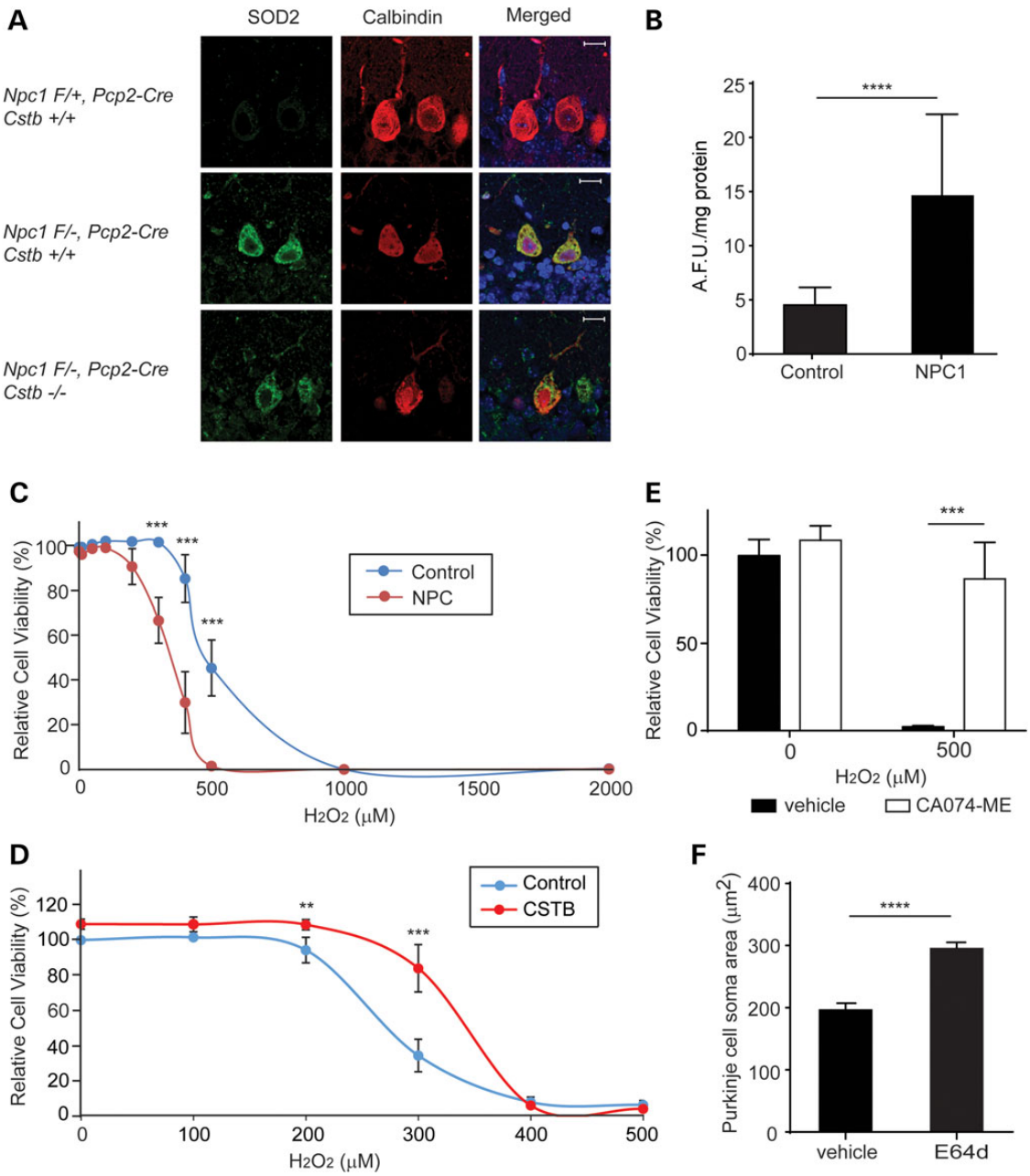

Figure 7. NPC1-deficient cells are more sensitive to oxidative damage and rescued by cathepsin B inhibition. (**A**) Immunofluorescence staining for SOD2 (green) and calbindin (red) at 3 weeks of age in the cerebellar midline; nuclei were stained by DAPI. Scale bar = 10 μm. (**B**) ROS levels were measured using 2,7-dichlorofluorescein diacetate (reported as arbitrary fluorescence units, AFU). Data are mean ± SD, $n = 3$ independent experiments, normalized to protein. $^{****}P < 0.0001$. (**C–E**) Viability of primary fibroblasts was determined by the XTT assay. Data are mean ± SD, $n = 3$ independent experiments, normalized to untreated control cells. $^{**}P < 0.01$ and $^{***}P < 0.001$. (C) Control and NPC1-deficient fibroblasts were treated with increasing concentrations (0–2000 μM) of H_2O_2 for 24 h. (D) NPC1-deficient fibroblasts were transfected to express CSTB or vector control. After 48 h, cells were treated with increasing concentrations of H_2O_2 for 24 h. (E) NPC1-deficient fibroblasts were treated concurrently with 0 or 500 μM H_2O_2 and with vehicle (DMSO) or 1 μM CA-074ME for 24 h. (**F**) Quantification of lobule IX Purkinje cell soma size in *Npc1-I1061T* homozygous mice treated with 10 mg/kg E64d or vehicle by daily oral gavage from 7 to 10 weeks (mean ± SEM, $n = 45$ cells per genotype, $^{****}P < 0.0001$).

our data are consistent with reports from NPC and NPA mouse models, in which enhanced cytosolic localization of cathepsins (26,27) and the occurrence of oxidative damage within the CNS (38,39) have been documented. Notably, a number of studies have demonstrated that cathepsins retain some activity at neutral pH (9–11). Furthermore, *in vitro* experiments performed at neutral pH demonstrate that cathepsins B, H, L, S and K cleave Bid and induce release of cytochrome c from isolated mitochondria, leading to the activation of caspases (36,55). Prior studies have also shown that cystatin B deficiency sensitizes neurons or tumor cells to oxidative stress (29,56), observations that are consistent with our model. We note that cystatin B may exert additional protective effects on the survival of Purkinje cells through alternative mechanisms. For example, cystatin B has been shown to protect mitochondrial integrity following exposure to ROS, independent of its action on lysosomal cathepsins (57). Accordingly, we can infer that cystatin B may exert beneficial effects on Purkinje cells by acting upon several distinct targets.

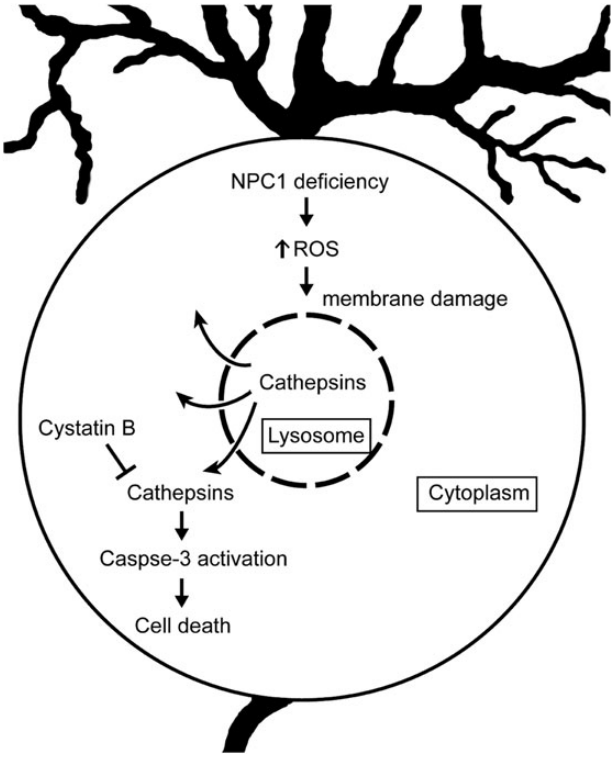

Figure 8. Model of Purkinje cell degeneration in NPC1 disease. NPC1 deficiency results in the increased production of ROS, which damage lysosomal membranes, promote leakage of cathepsins into the cytosol and lead to apoptotic death of Purkinje cells. Cystatin B functions to block this cascade by inhibiting cathepsins.

The exquisite sensitivity of Npc1-deficient Purkinje neurons to the effects of cystatin B deletion is noteworthy. To glean insights into this observation, we queried the Allen Brain Atlas, an online database that contains quantitative three-dimensional expression data derived from *in situ* hybridizations performed on the adult mouse brain. In this database, cystatin B expression is observed in the cerebellum, medulla and pons, whereas cathepsin B expression occurs widely throughout the CNS. In addition, reports indicate that most neurons in the adult rat cerebellum do not express detectable amounts of cystatin B, with the exception of Purkinje cells and some cells of the molecular layer of the cerebellar folia (58). In the human cerebellum, cystatin B is present in Purkinje cells and Bergmann glia (58). Thus, cystatin B may function as a vital inhibitor of cathepsins in cerebellar Purkinje cells, whereas other mechanisms predominate in many other brain regions. Additional factors may also contribute to Purkinje cell degeneration in double null mutant mice, such as increased sensitivity to ROS that leads to enhanced lysosomal membrane damage. Our studies offer insights into mechanisms underlying neuron loss in NPC disease and suggest potential strategies to ameliorate this process. Indeed, a cathepsin inhibitor has been shown to abrogate death of cortical neurons *in vitro* following treatment with U18666A, a small molecule that mimics the NPC phenotype by binding to NPC1 and inhibiting cholesterol efflux (26,59,60). These findings suggest that targeting the lysosomal cell death pathway may be beneficial in preventing neurodegeneration in NPC disease. Our data provide critical support that this pathogenic cascade underlies neuronal loss in NPC disease, an insight that provides a foundation for the future development of therapeutic strategies.

Materials and Methods

Reagents

Magic Red cathepsin B assay kit (cat. 938) was from Immunochemistry Technologies (Bloomington, MN, USA). E64d (sc-201280A) was from Santa Cruz (Dallas, TX). Fluorescent dextran (D3305) and BODIPY 493/503 (D3922) were from Life Technologies (Carlsbad, CA, USA). 2,7-Dichlorofluorescein diacetate (D6883), filipin (F9765) and all other chemicals were from Sigma-Aldrich (St. Louis, MO, USA). Antibodies used in this study were anti-NPC1 (Abcam, Cambridge, UK, ab36983), anti-GAPDH (Santa Cruz, sc-25578), anti-GFAP (Dako, Glostrup, Denmark, Z0334), anti-Iba1 (Wako, Osaka, Japan, 019-19741), anti-calbindin (Sigma-Aldrich, c2724), anti-cathepsin B (Abcam, ab33538), anti-cathepsin L (Athens Research and Technology, Athens, GA, 01-12-030112), anti-cystatin B (Sigma-Aldrich, C5243), anti-SOD-2 (Novus Biologicals, Littleton, CO, USA, NB100-1992) and anti-caspase-3 (Cell Signaling, Danvers, MA, USA, 9664). Anti-GM2 antibody was a gift from Dr Kostantin Dobrenis (Albert Einstein College of Medicine).

Mice

Mice containing the flox and null *Npc1* alleles and the *Pcp2-Cre* transgene were generated and genotyped as described previously (32). Mice with a cystatin B null allele were initially from Dr Richard Myers (31). Mice with an *Npc1-I1061T* knock-in allele were previously described (61). All lines were backcrossed to C57BL6/J for 10 or more generations. For E64d treatment, *Npc1-I1061T* homozygous mutant mice were treated by oral gavage daily for 3 weeks, from 7 to 10 weeks of age. E64d was suspended in dimethyl sulfoxide (DMSO) at 20 mg/ml. E64d or DMSO was diluted in saline buffer and administered at 10 mg/kg using a feeding tube. All animal procedures were approved by the University of Michigan Committee on the Use and Care of Animals.

Behavioral testing

Motor function was measured by the balance beam test. Mice at 7 weeks of age were trained on 3 consecutive days to cross a 6 mm wide beam suspended at 50 cm. Mice were then tested in triplicate at 8 weeks of age. Data are reported as average time to traverse the beam, allowing a maximum of 25 s and scoring falls as 25 s.

Filipin staining

Human fibroblasts (Coriell Cell Repositories, Camden, NJ, USA, control, GM08399; NPC1 P237S/I1061T, GM03123) were grown in chamber slides (Nunc, Lab-Tek, Penfield, NY, USA, 154526), rinsed with phosphate-buffered saline (PBS) and fixed with 4% paraformaldehyde for 30 min. After washing with PBS, cells were incubated with 1.5 mg/ml glycine for 10 min, washed with PBS and stained with 0.05 mg/ml filipin, 0.02 mg/ml BODIPY and 10% fetal bovine serum in PBS for 2 h at room temperature. Stained cells were imaged by focussing on the BODIPY channel. Filipin images were captured with the UV filter set on a Zeiss AxioImager Z1 microscope. Quantitative analysis of filipin images from more than five fields per experiment was performed by NIH ImageJ software, as described previously (62). Data reported are from three independent experiments. For mouse brain staining, tissue embedded in optimal cutting temperature (OCT) compound (Sakura, Tissue-Tek, Torrance, CA, USA) was sectioned at 10 μm and stained as described earlier. Representative images are from one of three mice per genotype.

Immunofluorescence staining

About 5 μm sections from brains embedded in paraffin were deparaffinized with xylenes and ethanol. Sections were boiled in 10 mM sodium citrate, pH 6, for 10 min for antigen retrieval. After washing with water, sections were blocked with 5% goat serum and 1% bovine serum albumin (BSA) in PBS for 1 h and then incubated in primary antibody (calbindin 1:500, LAMP1 1:10, cathepsin B 1:50, cathepsin L 1:100, GFAP 1:1000, Iba1 1:1000, caspase-3 1:200 and SOD-2 1:200) diluted in 1.5% blocking solution overnight at 4°C. Sections were subsequently incubated in secondary antibodies conjugated to Alexa Fluor 594 or 488 for 2 h and mounted with mounting medium including DAPI (Vector Lab, Burlingame, CA, USA, H-1200). Images were captured on an Olympus FluoView 500 Confocal microscope. Co-localization was quantified using Zeiss MetaMorph imaging software.

Gene knockdown

ON-TARGET plus SMART pool cystatin B siRNA (Dharmacon, Lafayette, CO, USA, L-017240-00-0005) and ON-TARGET plus non-targeting pool (Dharmacon, D-001810-10-05) were used to modulate gene expression. Cells were transfected with 10 μl of 10 μM siRNA using Nucleofector II (Lonza, Basel, Switzerland, program U-23), following the manufacturer's instructions.

Cathepsin B assay

Control or NPC1-deficient fibroblasts (GM03123) were transfected with siRNA as indicated in the figure legend, cultured in a chamber slide (Lab-Tek, 1554096) and analyzed for cathepsin B activity after 48 h, as described previously (6). Briefly, the cells were incubated with a 1:3000 dilution of cathepsin B-specific Magic Red reagent and imaged using a Deltavision-RT Live Cell Imaging System. Images were captured at 1 min intervals for 20 min. Fluorescence at 554/25 nm excitation and 609/25 nm emission was quantified using NIH ImageJ. Total fluorescence intensity above threshold was plotted as a function of time, and the slope of the line was used to determine cathepsin B activity.

Immunohistochemical staining

About 10 μm sections from brains embedded in OCT were boiled in 10 mM sodium citrate, pH 6, for 10 min. After washing with PBS, tissue sections were treated with 3% hydrogen peroxide for 10 min to quench endogenous peroxidase activity. Sections were blocked with 5% goat serum, 1% BSA, 0.02% saponin in PBS for 1 h and then stained overnight at 4°C with a GM2 antibody (1:15) diluted in 1.5% blocking solution. Sections were subsequently incubated with a biotinylated anti-mouse antibody (1:400) for 2 h at room temperature. Vectastain Avidin-Biotin Complex (ABC) reagent (Vector Lab, PK4001) and a peroxidase substrate (DAB) reagent (Vector Lab, SK4100) were used to detect the biotinylated secondary antibody. Representative images in the figure are from one of three mice per genotype.

Morphological analysis

Purkinje cell density and cerebellar area were quantified in midline sagittal sections stained with hematoxylin and eosin. For cell density, Purkinje cells were recognized as large cells with amphophilic cytoplasm, large nuclei with open chromatin and prominent nucleoli that were located between the molecular and granular layers. The number of cells was normalized to the length of the Purkinje layer, as measured by NIH ImageJ software. For cerebellar area, the cerebellum was selected and measured by NIH ImageJ, and pixel size was converted to μm^2 using the scale bar as a calibration standard. For analysis of Purkinje cell soma size, calbindin staining was used to define the cell soma. The area was measured as described earlier for analysis of cerebellar area.

Western blotting

Cells were lysed in RIPA buffer (Thermo Scientific, Waltham, MA, USA) containing Complete protease inhibitor (Roche, Basel, Switzerland) and Halt phosphatase inhibitor (Thermo Scientific). Protein concentrations were measured by the Bio-Rad DC protein assay kit (Bio-Rad, Hercules, CA, USA) and normalized. Proteins were separated by 4–20% gradient sodium dodecyl sulfate–polyacrylamide gel electrophoresis and transferred to nitrocellulose membranes using a semidry electrophoretic transfer apparatus (Bio-Rad). Immunoreactivity was detected by TMA-6 (Lumigen, Southfield, MI, USA) or ECL (Thermo Scientific). Antibodies used were anti-cathepsin B (1:500), anti-cystatin B (1:10 000), anti-GAPDH (1:5000) and anti-NPC1 (1:1000). Each protein band was selected and quantified by ImageJ software after subtracting the background signal. Specific band intensity was normalized to GAPDH.

Cell viability assay

Control or NPC1-deficient fibroblasts (Coriell, GM03123) were treated with the indicated doses of H_2O_2 for 24 h. Cell viability was determined by the XTT assay (ATCC, Manassas, VA, USA, 30–1011K), following the manufacturer's instructions. In brief, 50 μl of XTT was added in 100 μl cell culture medium and cells were incubated for 4 h in a CO_2 incubator at 37°C. The plates were measured in a microplate spectrophotometer at 490 nm for specific absorbance and at 650 nm for non-specific absorbance. For cystatin B overexpression, Nucleofector II (Lonza, program U-23) was used to transfect cells with the indicated plasmids. After 48 h, cells were treated with H_2O_2 for 24 h and tested for viability. To inhibit cathepsin B activity, 1 μM CA-074ME was used.

ROS measurement

Control and NPC1-deficient fibroblasts (Coriell, GM18453) were plated in six-well plates. After culturing for 1 day, cells were gently rinsed with PBS and treated with 50 μM 2,7-dichlorofluorescein diacetate. Following 1 h incubation, plates were measured in a fluorescence plate reader (excitation 485 nm and emission 527 nm). After reading, cells were rinsed with PBS, lysed in RIPA buffer and total protein measured by the BCA method.

Statistics

Statistical significance was assessed by unpaired Student's t-test (for comparison of two means) or analysis of variance (for comparison of more than two means). Statistics were performed using the Prism 6.02 software (GraphPad). $P < 0.05$ was considered significant.

Acknowledgements

We thank Dr Joel Swanson for insightful discussions, Drs Richard Myers and Ralph Nixon for *Cstb* null mice and Dr Kostantin Dobrenis for anti-GM2 antibody. We thank Brian Gregorka, Mark Schultz and Kelsey Krus for technical assistance.

Conflict of Interest statement. None declared.

Funding

This work was supported by the National Institutes of Health (R01 NS063967 to A.P.L.).

References

1. Settembre, C., Fraldi, A., Medina, D.L. and Ballabio, A. (2013) Signals from the lysosome: a control centre for cellular clearance and energy metabolism. *Nat. Rev. Mol. Cell Biol.*, **14**, 283–296.
2. de Duve, C. (2005) The lysosome turns fifty. *Nat. Cell Biol.*, **7**, 847–849.
3. Schultz, M.L., Tecedor, L., Chang, M. and Davidson, B.L. (2011) Clarifying lysosomal storage diseases. *Trends Neurosci.*, **34**, 401–410.
4. Nakanishi, H. (2003) Neuronal and microglial cathepsins in aging and age-related diseases. *Ageing Res. Rev.*, **2**, 367–381.
5. Yamashima, T. (2000) Implication of cysteine proteases calpain, cathepsin and caspase in ischemic neuronal death of primates. *Prog. Neurobiol.*, **62**, 273–295.
6. Elrick, M.J., Yu, T., Chung, C. and Lieberman, A.P. (2012) Impaired proteolysis underlies autophagic dysfunction in Niemann-Pick type C disease. *Hum. Mol. Genet.*, **21**, 4876–4887.
7. Pislar, A. and Kos, J. (2014) Cysteine cathepsins in neurological disorders. *Mol. Neurobiol.*, **49**, 1017–1030.
8. Katunuma, N. (2010) Posttranslational processing and modification of cathepsins and cystatins. *J. Signal. Transduct.*, 2010, 375345.
9. Turk, B., Bieth, J.G., Bjork, I., Dolenc, I., Turk, D., Cimerman, N., Kos, J., Colic, A., Stoka, V. and Turk, V. (1995) Regulation of the activity of lysosomal cysteine proteinases by pH-induced inactivation and/or endogenous protein inhibitors, cystatins. *Biol. Chem. Hoppe Seyler*, **376**, 225–230.
10. Turk, B., Dolenc, I., Turk, V. and Bieth, J.G. (1993) Kinetics of the pH-induced inactivation of human cathepsin L. *Biochemistry*, **32**, 375–380.
11. Turk, B., Dolenc, I., Zerovnik, E., Turk, D., Gubensek, F. and Turk, V. (1994) Human cathepsin B is a metastable enzyme stabilized by specific ionic interactions associated with the active site. *Biochemistry*, **33**, 14800–14806.
12. Groth-Pedersen, L. and Jaattela, M. (2013) Combating apoptosis and multidrug resistant cancers by targeting lysosomes. *Cancer Lett.*, **332**, 265–274.
13. Turk, V. and Bode, W. (1991) The cystatins: protein inhibitors of cysteine proteinases. *FEBS Lett.*, **285**, 213–219.
14. Vanier, M.T. (2013) Niemann-Pick diseases. *Handb. Clin. Neurol.*, **113**, 1717–1721.
15. Carstea, E.D., Morris, J.A., Coleman, K.G., Loftus, S.K., Zhang, D., Cummings, C., Gu, J., Rosenfeld, M.A., Pavan, W.J., Krizman, D.B. *et al.* (1997) Niemann-Pick C1 disease gene: homology to mediators of cholesterol homeostasis. *Science*, **277**, 228–231.
16. Naureckiene, S., Sleat, D.E., Lackland, H., Fensom, A., Vanier, M.T., Wattiaux, R., Jadot, M. and Lobel, P. (2000) Identification of HE1 as the second gene of Niemann-Pick C disease. *Science*, **290**, 2298–2301.
17. Infante, R.E., Wang, M.L., Radhakrishnan, A., Kwon, H.J., Brown, M.S. and Goldstein, J.L. (2008) NPC2 facilitates bidirectional transfer of cholesterol between NPC1 and lipid bilayers, a step in cholesterol egress from lysosomes. *Proc. Natl Acad. Sci. USA*, **105**, 15287–15292.
18. Kwon, H.J., Abi-Mosleh, L., Wang, M.L., Deisenhofer, J., Goldstein, J.L., Brown, M.S. and Infante, R.E. (2009) Structure of N-terminal domain of NPC1 reveals distinct subdomains for binding and transfer of cholesterol. *Cell*, **137**, 1213–1224.
19. Elrick, M.J. and Lieberman, A.P. (2013) Autophagic dysfunction in a lysosomal storage disorder due to impaired proteolysis. *Autophagy*, **9**, 234–235.
20. Sarkar, S., Carroll, B., Buganim, Y., Maetzel, D., Ng, A.H., Cassady, J.P., Cohen, M.A., Chakraborty, S., Wang, H., Spooner, E. *et al.* (2013) Impaired autophagy in the lipid-storage disorder Niemann-Pick type C1 disease. *Cell Rep.*, **5**, 1302–1315.
21. Lieberman, A.P., Puertollano, R., Raben, N., Slaugenhaupt, S., Walkley, S.U. and Ballabio, A. (2012) Autophagy in lysosomal storage disorders. *Autophagy*, **8**, 719–730.
22. Pacheco, C.D., Kunkel, R. and Lieberman, A.P. (2007) Autophagy in Niemann–Pick C disease is dependent upon Beclin-1 and responsive to lipid trafficking defects. *Hum. Mol. Genet.*, **16**, 1495–1503.
23. Higashi, Y., Murayama, S., Pentchev, P.G. and Suzuki, K. (1993) Cerebellar degeneration in the Niemann-Pick type C mouse. *Acta Neuropathol.*, **85**, 175–184.
24. Liao, G., Yao, Y., Liu, J., Yu, Z., Cheung, S., Xie, A., Liang, X. and Bi, X. (2007) Cholesterol accumulation is associated with lysosomal dysfunction and autophagic stress in Npc1−/− mouse brain. *Am. J. Pathol.*, **171**, 962–975.
25. Ordonez, M.P., Roberts, E.A., Kidwell, C.U., Yuan, S.H., Plaisted, W.C. and Goldstein, L.S. (2012) Disruption and therapeutic rescue of autophagy in a human neuronal model of Niemann Pick type C1. *Hum. Mol. Genet.*, **21**, 2651–2662.
26. Amritraj, A., Peake, K., Kodam, A., Salio, C., Merighi, A., Vance, J.E. and Kar, S. (2009) Increased activity and altered subcellular distribution of lysosomal enzymes determine neuronal vulnerability in Niemann-Pick type C1-deficient mice. *Am. J. Pathol.*, **175**, 2540–2556.
27. Gabande-Rodriguez, E., Boya, P., Labrador, V., Dotti, C.G. and Ledesma, M.D. (2014) High sphingomyelin levels induce lysosomal damage and autophagy dysfunction in Niemann Pick disease type A. *Cell Death Differ.*, **21**, 864–875.
28. Yang, D.S., Stavrides, P., Mohan, P.S., Kaushik, S., Kumar, A., Ohno, M., Schmidt, S.D., Wesson, D., Bandyopadhyay, U., Jiang, Y. *et al.* (2011) Reversal of autophagy dysfunction in the TgCRND8 mouse model of Alzheimer's disease ameliorates amyloid pathologies and memory deficits. *Brain*, **134**, 258–277.
29. Butinar, M., Prebanda, M.T., Rajkovic, J., Jeric, B., Stoka, V., Peters, C., Reinheckel, T., Kruger, A., Turk, V., Turk, B. *et al.* (2014) Stefin B deficiency reduces tumor growth via sensitization of tumor cells to oxidative stress in a breast cancer model. *Oncogene*, **33**, 3392–3400.
30. Chang, S.H., Kanasaki, K., Gocheva, V., Blum, G., Harper, J., Moses, M.A., Shih, S.C., Nagy, J.A., Joyce, J., Bogyo, M. *et al.* (2009) VEGF-A induces angiogenesis by perturbing the cathepsin–cysteine protease inhibitor balance in venules, causing basement membrane degradation and mother vessel formation. *Cancer Res.*, **69**, 4537–4544.
31. Pennacchio, L.A., Bouley, D.M., Higgins, K.M., Scott, M.P., Noebels, J.L. and Myers, R.M. (1998) Progressive ataxia, myoclonic epilepsy and cerebellar apoptosis in cystatin B-deficient mice. *Nat. Genet.*, **20**, 251–258.
32. Elrick, M.J., Pacheco, C.D., Yu, T., Dadgar, N., Shakkottai, V.G., Ware, C., Paulson, H.L. and Lieberman, A.P. (2010) Conditional Niemann-Pick C mice demonstrate cell autonomous Purkinje cell neurodegeneration. *Hum. Mol. Genet.*, **19**, 837–847.
33. Barski, J.J., Dethleffsen, K. and Meyer, M. (2000) Cre recombinase expression in cerebellar Purkinje cells. *Genesis*, **28**, 93–98.

34. Brunk, U.T., Dalen, H., Roberg, K. and Hellquist, H.B. (1997) Photo-oxidative disruption of lysosomal membranes causes apoptosis of cultured human fibroblasts. *Free Radic. Biol. Med.*, **23**, 616–626.
35. Boya, P., Andreau, K., Poncet, D., Zamzami, N., Perfettini, J.L., Metivier, D., Ojcius, D.M., Jaattela, M. and Kroemer, G. (2003) Lysosomal membrane permeabilization induces cell death in a mitochondrion-dependent fashion. *J. Exp. Med.*, **197**, 1323–1334.
36. Cirman, T., Oresic, K., Mazovec, G.D., Turk, V., Reed, J.C., Myers, R.M., Salvesen, G.S. and Turk, B. (2004) Selective disruption of lysosomes in HeLa cells triggers apoptosis mediated by cleavage of Bid by multiple papain-like lysosomal cathepsins. *J. Biol. Chem.*, **279**, 3578–3587.
37. Kagedal, K., Zhao, M., Svensson, I. and Brunk, U.T. (2001) Sphingosine-induced apoptosis is dependent on lysosomal proteases. *Biochem. J.*, **359**, 335–343.
38. Zampieri, S., Mellon, S.H., Butters, T.D., Nevyjel, M., Covey, D.F., Bembi, B. and Dardis, A. (2009) Oxidative stress in NPC1 deficient cells: protective effect of allopregnanolone. *J. Cell. Mol. Med.*, **13**, 3786–3796.
39. Vazquez, M.C., Balboa, E., Alvarez, A.R. and Zanlungo, S. (2012) Oxidative stress: a pathogenic mechanism for Niemann-Pick type C disease. *Oxid. Med. Cell. Longev.*, 2012, 205713.
40. Porter, F.D., Scherrer, D.E., Lanier, M.H., Langmade, S.J., Molugu, V., Gale, S.E., Olzeski, D., Sidhu, R., Dietzen, D.J., Fu, R. *et al.* (2010) Cholesterol oxidation products are sensitive and specific blood-based biomarkers for Niemann-Pick C1 disease. *Sci. Transl. Med.*, **2**, 56ra81.
41. Fu, R., Wassif, C.A., Yanjanin, N.M., Watkins-Chow, D.E., Baxter, L.L., Incao, A., Liscum, L., Sidhu, R., Firnkes, S., Graham, M. *et al.* (2013) Efficacy of N-acetylcysteine in phenotypic suppression of mouse models of Niemann-Pick disease, type C1. *Hum. Mol. Genet.*, **22**, 3508–3523.
42. Terman, A., Kurz, T., Gustafsson, B. and Brunk, U.T. (2006) Lysosomal labilization. *IUBMB Life*, **58**, 531–539.
43. Krenn, M.A., Schurz, M., Teufl, B., Uchida, K., Eckl, P.M. and Bresgen, N. (2015) Ferritin-stimulated lipid peroxidation, lysosomal leak, and macroautophagy promote lysosomal 'metastability' in primary hepatocytes determining *in vitro* cell survival. *Free Radic. Biol. Med.*, **80**, 48–58.
44. Zhao, M., Antunes, F., Eaton, J.W. and Brunk, U.T. (2003) Lysosomal enzymes promote mitochondrial oxidant production, cytochrome c release and apoptosis. *Eur. J. Biochem./FEBS*, **270**, 3778–3786.
45. Buttle, D.J., Murata, M., Knight, C.G. and Barrett, A.J. (1992) CA074 methyl ester: a proinhibitor for intracellular cathepsin B. *Arch. Biochem. Biophys.*, **299**, 377–380.
46. Towatari, T., Nikawa, T., Murata, M., Yokoo, C., Tamai, M., Hanada, K. and Katunuma, N. (1991) Novel epoxysuccinyl peptides. A selective inhibitor of cathepsin B, *in vivo*. *FEBS Lett.*, **280**, 311–315.
47. Yamamoto, A., Kaji, T., Tomoo, K., Ishida, T., Inoue, M., Murata, M. and Kitamura, K. (1992) Crystallization and preliminary X-ray study of the cathepsin B complexed with CA074, a selective inhibitor. *J. Mol. Biol.*, **227**, 942–944.
48. Luo, C.L., Chen, X.P., Yang, R., Sun, Y.X., Li, Q.Q., Bao, H.J., Cao, Q.Q., Ni, H., Qin, Z.H. and Tao, L.Y. (2010) Cathepsin B contributes to traumatic brain injury-induced cell death through a mitochondria-mediated apoptotic pathway. *J. Neurosci. Res.*, **88**, 2847–2858.
49. Hook, V., Kindy, M. and Hook, G. (2007) Cysteine protease inhibitors effectively reduce *in vivo* levels of brain beta-amyloid related to Alzheimer's disease. *Biol. Chem.*, **388**, 247–252.
50. Hook, V.Y., Kindy, M. and Hook, G. (2008) Inhibitors of cathepsin B improve memory and reduce beta-amyloid in transgenic Alzheimer disease mice expressing the wild-type, but not the Swedish mutant, beta-secretase site of the amyloid precursor protein. *J. Biol. Chem.*, **283**, 7745–7753.
51. Xu, M., Yang, L., Rong, J.G., Ni, Y., Gu, W.W., Luo, Y., Ishidoh, K., Katunuma, N., Li, Z.S. and Zhang, H.L. (2014) Inhibition of cysteine cathepsin B and L activation in astrocytes contributes to neuroprotection against cerebral ischemia via blocking the tBid-mitochondrial apoptotic signaling pathway. *Glia*, **62**, 855–880.
52. McGowan, E.B., Becker, E. and Detwiler, T.C. (1989) Inhibition of calpain in intact platelets by the thiol protease inhibitor E-64d. *Biochem. Biophys. Res. Commun.*, **158**, 432–435.
53. Hook, G., Hook, V. and Kindy, M. (2011) The cysteine protease inhibitor, E64d, reduces brain amyloid-beta and improves memory deficits in Alzheimer's disease animal models by inhibiting cathepsin B, but not BACE1, beta-secretase activity. *J. Alzheimers Dis.*, **26**, 387–408.
54. Hook, G.R., Yu, J., Sipes, N., Pierschbacher, M.D., Hook, V. and Kindy, M.S. (2014) The cysteine protease cathepsin B is a key drug target and cysteine protease inhibitors are potential therapeutics for traumatic brain injury. *J. Neurotrauma*, **31**, 515–529.
55. Taylor, R.C., Cullen, S.P. and Martin, S.J. (2008) Apoptosis: controlled demolition at the cellular level. *Nat. Rev. Mol. Cell Biol.*, **9**, 231–241.
56. Lehtinen, M.K., Tegelberg, S., Schipper, H., Su, H., Zukor, H., Manninen, O., Kopra, O., Joensuu, T., Hakala, P., Bonni, A. *et al.* (2009) Cystatin B deficiency sensitizes neurons to oxidative stress in progressive myoclonus epilepsy, EPM1. *J. Neurosci.*, **29**, 5910–5915.
57. Maher, K., Jeric Kokelj, B., Butinar, M., Mikhaylov, G., Mancek-Keber, M., Stoka, V., Vasiljeva, O., Turk, B., Grigoryev, S.A. and Kopitar-Jerala, N. (2014) A role for stefin B (cystatin B) in inflammation and endotoxemia. *J. Biol. Chem.*, **289**, 31736–31750.
58. Riccio, M., Santi, S., Dembic, M., Di Giaimo, R., Cipollini, E., Costantino-Ceccarini, E., Ambrosetti, D., Maraldi, N.M. and Melli, M. (2005) Cell-specific expression of the epm1 (cystatin B) gene in developing rat cerebellum. *Neurobiol. Dis.*, **20**, 104–114.
59. Liscum, L. and Faust, J.R. (1989) The intracellular transport of low density lipoprotein-derived cholesterol is inhibited in Chinese hamster ovary cells cultured with 3-beta-[2-(diethylamino)ethoxy]androst-5-en-17-one. *J. Biol. Chem.*, **264**, 11796–11806.
60. Lu, F., Liang, Q., Abi-Mosleh, L., Das, A., De Brabander, J.K., Goldstein, J.L. and Brown, M.S. (2015) Identification of NPC1 as the target of U18666A, an inhibitor of lysosomal cholesterol export and Ebola infection. *eLife*, **4**, doi: 10.7554/eLife.12177.
61. Praggastis, M., Tortelli, B., Zhang, J., Fujiwara, H., Sidhu, R., Chacko, A., Chen, Z. and Chung, C. (2015) A murine Niemann-Pick C1 I1061T knock-in model recapitulates the pathological features of the most prevalent human disease allele. *J. Neurosci.*, **35**, 8091–8106.
62. Yu, T., Chung, C., Shen, D., Xu, H. and Lieberman, A.P. (2012) Ryanodine receptor antagonists adapt NPC1 proteostasis to ameliorate lipid storage in Niemann-Pick type C disease fibroblasts. *Hum. Mol. Genet.*, **21**, 3205–3214.